

Spatial structure of the dominant basin-scale internal waves in Lake Kinneret

Andrés Gómez-Giraldo,¹ Jörg Imberger, and Jason P. Antenucci

Centre for Water Research, University of Western Australia, Crawley 6009, Western Australia, Australia

Abstract

Field data and numerical simulations were used to investigate the effects of basin shape, continuous stratification, and rotation on the three-dimensional structure of the dominant natural basin-scale internal-wave modes in Lake Kinneret, a stratified lake large enough so that the earth's rotation influences the wave motion. The structure of the modes was inferred from power spectral density of measured and simulated isotherm vertical displacements and from rotary-power spectral density of isopycnal velocities obtained from numerical simulations. The shape of the lake at the level of the thermocline, in conjunction with the dispersion relationship, determines the horizontal configuration of the natural modes. The dominant response to wind forcing was an azimuthal and vertical mode 1 Kelvin wave with a natural period of 22.6 h that propagated around the entire basin; the second most dominant response was a vertical mode 1 wave with a natural period close to 10.5 h and composed of two counter-rotating Poincaré circular cells. The sloping bottom produced an intensification of vertical displacements and velocities over the slope due to focusing of waves rays after reflection at bottom slopes close to the critical angle. The amplitude of the observed oscillations was very sensitive to the phase of the wind relative to the existing waves; resonance was affected by the cessation time of the wind events because it defines the local forcing period and resets the phase of the observed oscillations.

Basin-scale internal waves are ubiquitous to stratified lakes and reservoirs and drive a variety of physical, chemical, and biological processes in such water bodies (Mortimer 1974). They possess most of the energy contained in the internal wave spectrum and play an important role in energizing both vertical mixing and horizontal dispersion. Vertical mixing at the metalimnion level erodes the natural barrier imposed by the stratification and facilitates primary production in the surface layer by incorporating nutrient-rich hypolimnetic waters (e.g., Ostrovsky et al. 1996) into the surface layer. Energy is transferred from the basin-scale waves to turbulent mixing by sloshing and breaking of basin-scale internal waves around the perimeter of the lake, by the increased shear in the interior of the lake, or by the cascade of energy from the basin-scale waves to high-frequency internal waves that are generated either by nonlinear steepening or by shear instabilities (Imberger 1998; Boegman et al. 2003). Equally, basin-scale internal waves, combined with the action of the surface-wind-induced currents, sustain horizontal dispersion via a host of mechanisms: pseudo-chaotic dispersion (Stocker and Imberger 2003a), horizontal shear dispersion (Stocker and Imberger 2003b), and dispersion by synoptic eddies formed when internal Kelvin waves separate at headlands (Ivey and Maxworthy 1992). In addition,

the oscillating motion over a lake bed generates resuspension and transport of sediments, nutrients, and contaminants (Gloor et al. 1994). An understanding of the temporal and spatial patterns of the basin-scale internal waves is therefore necessary to better quantify the above processes that, in turn, determine the success of any water-quality investigation.

Observations of temperature or velocity fluctuations reveal that basin-scale internal waves have characteristic dominant periods, even when generated by isolated wind events or by wind forcing with different periods (Lemmin 1987; Saggio and Imberger 1998). The observations also show that the oscillations form coherent structures along vertical profiles and horizontal transects with length scales of the order of the dimensions of the basin (Thorpe 1974; Münnich et al. 1992; Hodges et al. 2000). This suggests that lakes are dynamic systems with natural (or free) modes of oscillations that have characteristic period and spatial structure and that a knowledge of the characteristics of these modes is crucial for understanding the baroclinic response of lakes to general forcing.

When the relative importance of Coriolis to buoyancy forces is small, as in low-latitude or narrow lakes, natural modes are nonrotating seiches and, when it is large, as in large lakes, the natural modes are rotating Kelvin and Poincaré waves (Mortimer 1974). In either case, the period and the spatial structure of the natural modes are also functions of the shape and the stratification of the lake. Analytical solutions for these functions have not been found for general bathymetries and only approximate solutions exist. Models with simple horizontal geometries (e.g., rectangular, circular, elliptical) and flat bottoms reproduce the periods well and give indications of the horizontal structure of the natural modes for layered (Heaps and Ramsbottom 1966; Csanady 1967; Antenucci and Imberger 2001) or for continuous stratifications (Csanady 1972; Turner 1973; Monismith 1987), but reveal little as to the effect of an irregular basin shape or a sloping bottom.

¹ Corresponding author (gomez-gi@cwr.uwa.edu.au).

Acknowledgments

The field experiment was funded by the Israeli Water Commission, via the Kinneret modeling project, conducted jointly by the Kinneret Limnological Laboratory (KLL) and the Centre for Water Research (CWR). Credits for the success of the field campaign go to the Field Operations Group at CWR and to the KLL laboratory. The authors thank the constructive and opportune comments by Erich Bäuerle, Greg Ivey, Geoff Wake, Kevin Lamb, and two reviewers. The first author gratefully acknowledges the support of an International Postgraduate Research Scholarship and an ad-hoc CWR scholarship. This article is Centre for Water Research contribution ED 1671 AG.

More elaborated numerical eigenvalue models allow mode determination considering a variable depth, but the stratification must be approximated by a series of homogeneous layers (Schwab 1977; Salvadè et al. 1988; Bäuerle 1998). Such numerical schemes yield horizontal structure of the pycnocline displacements closer to those observed, but the vertical structure of the modes is poorly reproduced. In particular, the changes of wave number, energy density, and amplitude of the wave beam on reflection from a sloping bottom (Phillips 1966; Eriksen 1982; Dauvois and Young 1999) cannot be captured by this type of model.

The structure of natural modes in a basin with a sloping bottom and a continuous stratification was studied numerically by Münnich (1996) and Fricker and Nepf (2000) for nonrotating, vertically two-dimensional basins with variable depth. They showed that the sloping bottom dramatically changes the spatial structure of the natural modes compared with those solutions obtained for a rectangular basin. Fricker and Nepf (2000) pointed out that an extension of their procedure to three dimensions (3-D) would be difficult.

Simulations with 3-D hydrodynamic models can reveal features that can be attributed to the spatial structure of the natural modes of oscillation. Rueda et al. (2003) associated features in the horizontal distribution of the integrated potential and kinetic energy of the vertical mode 1, basin-scale waves in Lake Tahoe with major lake boundary irregularities. The difficulty in using 3-D modeling to infer the shape and period of natural modes of oscillation is that, in general, it is difficult to isolate and interpret their characteristic features when the lake is constantly forced by an unsteady surface wind stress.

In Lake Kinneret (Israel), 24- and 12-h-period signals dominate the power spectra of the observed isotherm displacement and horizontal velocity (Serruya 1975; Ou and Bennett 1979; Antenucci et al. 2000). Serruya (1975) attributed the existence of these periodic motions to the interaction of the periodic wind with a 12-h natural period of oscillation, and documented the cyclonic rotation of the 24-h-period component of the signal. Ou and Bennett (1979) described the 24-h-period oscillation as a vertical and horizontal mode 1 (V1H1) Kelvin wave, and suggested that the 12-h-period motion was a nonrotating V1H1 seiche with a nodal line in the north–south direction. With the circular flat-bottom basin model approximation (Csanady 1967), Antenucci et al. (2000) estimated the period of the natural internal modes in Lake Kinneret to be 22.5 and 12.2 h and interpreted these as V1H1 cyclonic Kelvin and anticyclonic Poincaré waves, respectively. The proximity to the periods observed in the field led them to suggest that these two waves were the dominant modes in the lake. In a later article, Antenucci and Imberger (2003) showed how these modes moved in and out of resonance with the 24-h wind forcing as the stratification changed over a seasonal time scale (we refer to resonance as the amplification of the motion that occurs when the period and spatial structure of the forcing coincide with those of one of the natural modes of the system, and not in the sense used by Maas and Lam [1995], who called a resonance the condition in which all wave rays close upon themselves after multiple reflections at the boundaries of the domain). The numerical simulations of

Hodges et al. (2000) confirmed the rotational character of the 24-h component, but they attributed the 12-h component to a seiche across the east–west axis of the lake with a small north–south component. The conflicting results from these studies indicate that the 12-h component remains to be unequivocally characterized. Also, the dependence of the modal structure on the bathymetric shape, which is of critical importance in determining the bottom and metalimnetic shear-stress distribution, remains to be determined.

To address these issues, a field campaign was undertaken during a typical summer stratification period. After describing the field campaign, we illustrate the effects of the horizontal shape and sloping bottom of the basin on the structure of the dominant natural modes by using spectral analysis of field data and results of complementary numerical simulations. We also estimate their natural periods and show that the wind resets the phase of the observed wave field, imposing the observed periods, and that the time of termination of the wind events is a very important parameter for the observed resonant interaction with the wave field.

Field site

Lake Kinneret is a warm, monomictic lake, with the turnover occurring in late December or early January. The summer stratification is characterized by a thermocline 16 m deep and a temperature difference between the epilimnion and the hypolimnion of up to 8°C (Serruya 1975). The lake is approximately 22 km long north–south and 15 km wide west–east and the maximum depth was about 39 m during the summer of 2001, when the field experiment for this research was conducted (see Fig. 1). During the stratified condition, when internal wave activity is strongest, the dominant component of the wind forcing is a strong westerly breeze that blows every afternoon (Serruya 1975). Inflows, outflows, and density variation due to salinity have a negligible effect on the dynamics at this time of the year.

Field equipment

To record the internal waves activity, 10 Lake Diagnostic Systems (LDSs), containing thermistor chains and wind velocity sensors, were deployed in Lake Kinneret during the summer of 2001. Five of the LDSs were located close together to identify the characteristics of short-wavelength internal waves and the results from these chains will be described elsewhere; only data from one of these stations (Tv) is considered here. The location of the six LDS stations used for the present analysis is shown in Fig. 1, and details of their deployment are given in Table 1. The accuracy of the thermistors was 0.01°C (with resolution of 0.001°C). Stations Ty (one of the stations close to Tv) and T9 also had full meteorological stations mounted 1.5 m above the water surface.

Observed wind pattern

Each day during the experiment, westerly winds started abruptly after midday, reached speeds up to 11 m s⁻¹ that

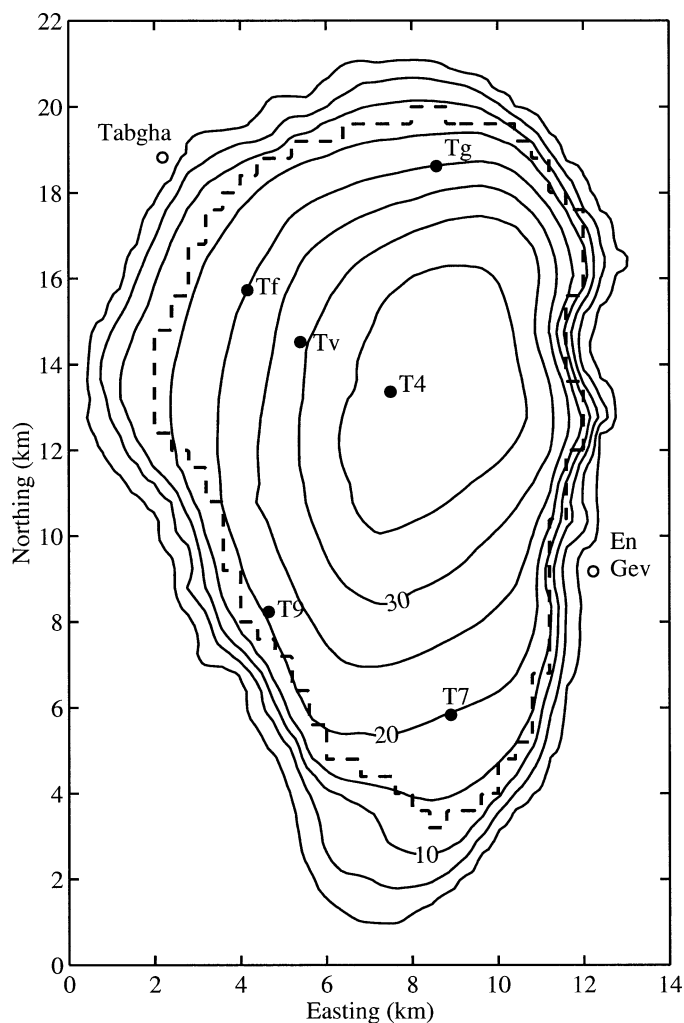


Fig. 1. Bathymetry of Lake Kinneret. Filled and open dots indicate the locations of LDS and external wind stations. The dashed contour indicates the perimeter of the flat-bottom basin used in one of the simulations. The origin of the map coordinate system is situated at 35.51°N, 32.70°E.

were maintained for 6–8 h (Fig. 2a,b), similar to that observed previously by Serruya (1975). Power spectral density (PSD; Bendat and Piersol 1986) of the wind speed (Fig. 2c) reveals that, in addition to the dominant 24-h periodicity, the wind signal contained a secondary 12-h periodic component that had also been identified by Ou and Bennett (1979) and Antenucci and Imberger (2003) in previous field campaigns. The spatial variability of the wind field during the 2001 field

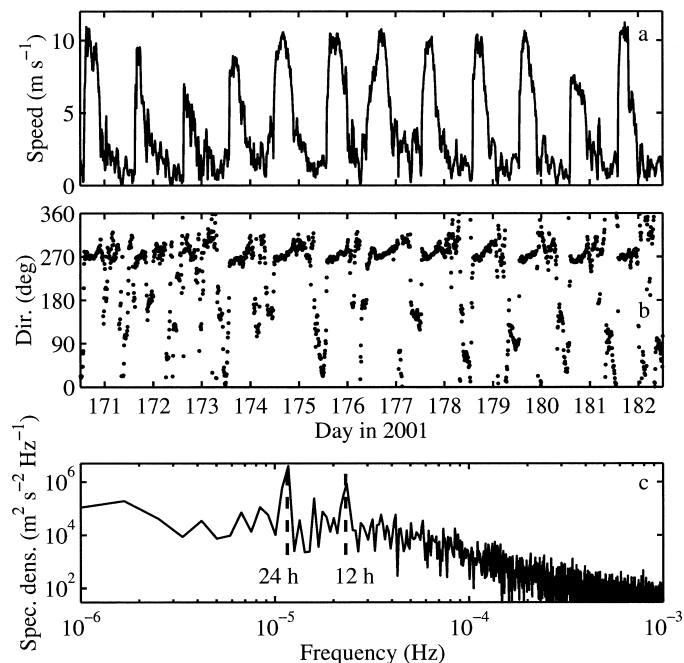


Fig. 2. (a) Wind speed and (b) wind direction (meteorological convention) measured 1.5 m over the lake surface at station Tv. (c) Power spectral density of the wind speed in (a).

experiment was documented by Laval et al. (2003b); the effects of the daily variations in the wind pattern are discussed below.

Measured basin-scale internal waves activity

The isotherm displacements (Fig. 3) and the PSD of the vertical displacement of the 23°C isotherm (Fig. 4), located in the middle of the metalimnion, show that a 24-h-period oscillation was dominant at all stations. This oscillation was more energetic at the stations located along the 20-m-depth contour (stations Tg, Tf, T7, and T9) and progressively less energetic toward the interior of the lake (stations Tv and T4). The second most energetic peak corresponds to a 12-h-period oscillation, which was larger at stations Tf, T9, and Tv and just significant at stations Tg, T7, and T4. The mean stratification in which these waves propagated was obtained by averaging the elevation of the isotherms at station T4 over 24 h from day 170.5 to 171.5 and is shown in Fig. 5 together with the corresponding buoyancy frequency profile. The buoyancy frequency was everywhere, even in the relatively well-mixed epilimnion and hypolimnion, three orders

Table 1. Details of the deployment.

Station	Deployment period	Depth (m)	Sampling interval (s)	Depth of thermistors
T4	01 Jan to 05 Jul	39.0	20	0.5 m and every 2 m from 2 m
Tg	22 Apr to 20 Jul	19.9	10	every 0.75 m from 0.75 m
Tf	22 Apr to 19 Jul	19.9	10	every 0.75 m from 0.75 m
T7	22 Apr to 20 Jul	20.3	10	every 0.75 m from 0.75 m
Tv	18 Jun to 02 Jul	29.5	10	every 0.75 m from 0.75 m
T9	17 Jun to 02 Jul	20.2	10	every 0.75 m from 0.75 m

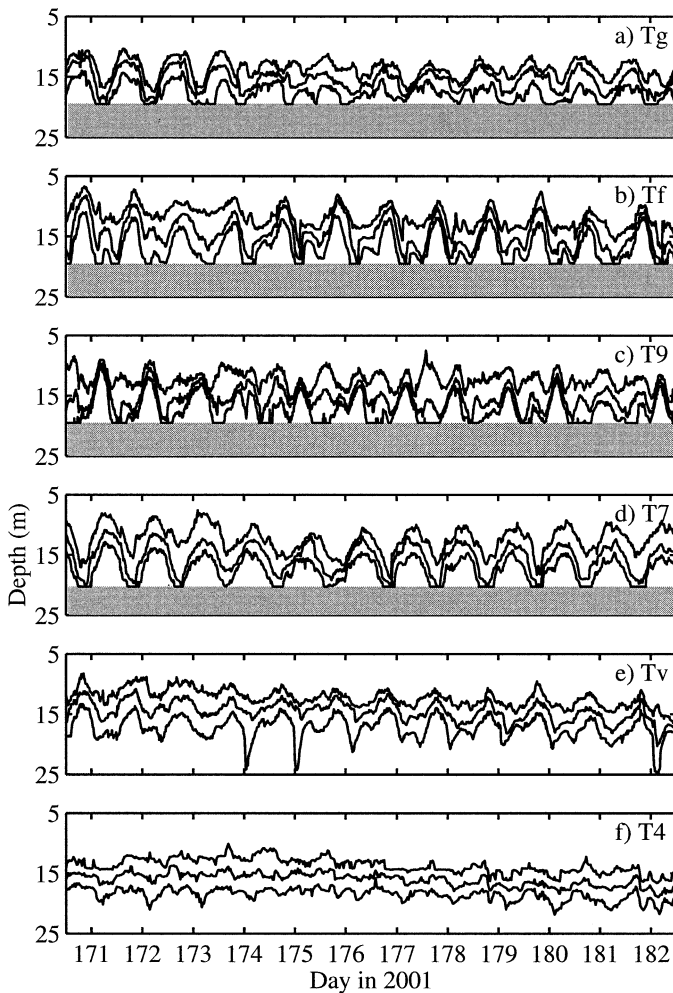


Fig. 3. Record of isotherm displacements. In each panel, the isotherms are 26°C, 23°C, and 20°C from top to bottom. Isotherm depths were determined through linear interpolation of temperature records at fixed depths. (a) Tg, (b) Tf, (c) T9, (d) T7, (e) Tv, and (f) T4.

of magnitude larger than the frequencies of the two dominant oscillatory motions (1×10^{-5} and 2×10^{-5} Hz). Therefore, the thermocline did not form a wave guide with turning levels and the corresponding wave rays could propagate in the entire lake from the surface to the bottom. The horizontal variation of the time-averaged temperature profile and any associated consequences could not be investigated because the metalimnion intercepts the bottom of the lake at the location of the stations Tg, Tf, T9, and T7.

Propagation—The propagation of the 24- and 12-h-period waves along the perimeter of the basin was tracked by following their phase at the stations located along the 20-m-depth contour. To do so, the displacement of the 23°C isotherm at each of the stations (Fig. 6a) was band-pass filtered around 24 h (between 19.8 and 27.8 h; Fig. 6b) and around 12 h (between 10.7 and 13.9 h; Fig. 6c) using a fourth-order Butterworth filter. The crests of the 24-h-period signal is seen to propagate cyclonically (anticlockwise) with oscillations at Tg and T7, located at opposite ends of the basin,

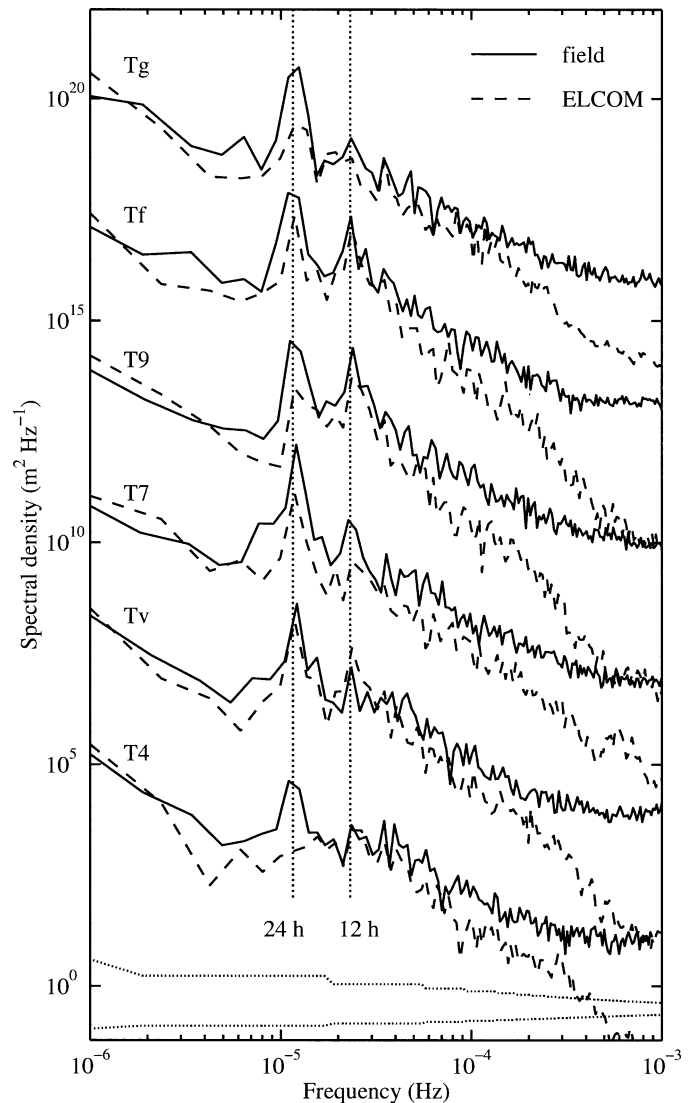


Fig. 4. Power spectra of measured and simulated vertical displacement of the 23°C isotherm. Spectra have been smoothed in the frequency domain to improve confidence. The two dotted lines near the bottom define confidence at the 95% level. Vertical dotted lines mark periods of 24 and 12 h. Offset is three logarithmic cycles.

perfectly out of phase, a characteristic of a basin-long azimuthal mode 1 wave. By contrast, the 12-h oscillation propagated anticyclonically (clockwise; Fig. 6c), but the oscillations were almost in phase at stations Tg and T7. This suggests that this oscillation did not correspond to a monocellular anticyclonic wave of the first azimuthal mode filling the entire basin, as postulated by Antenucci et al. (2000). It is possible that wave crests propagated along the transect T9–Tf–Tg while crests at T7 followed a disconnected path. A different line type is used in Fig. 6c to indicate that the propagation of wave crests between T7 and T9 was questionable.

Azimuthal structure—We studied the azimuthal structure of the dominant components of the wave field by looking at the evolution, over a period of 24 h, of the band-passed

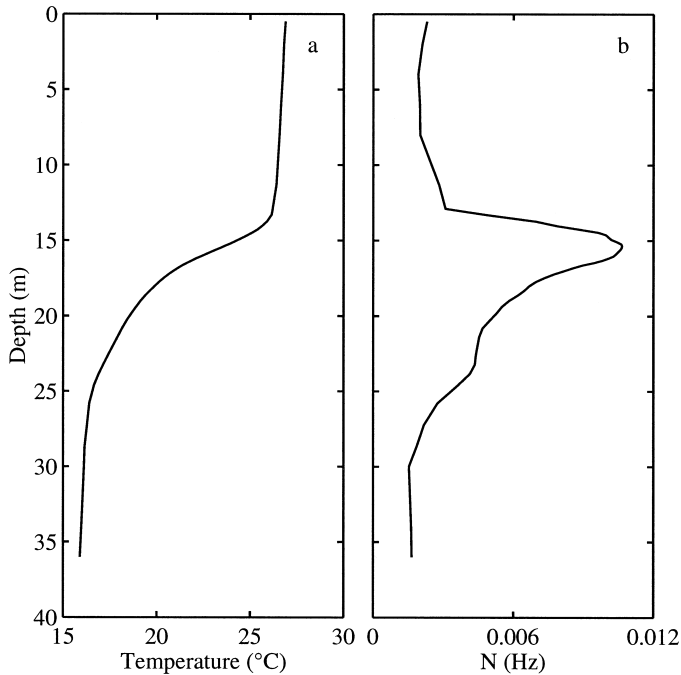


Fig. 5. (a) Mean temperature profile at station T4 for days 170.5–171.5 in 2001. (b) Associated buoyancy frequency.

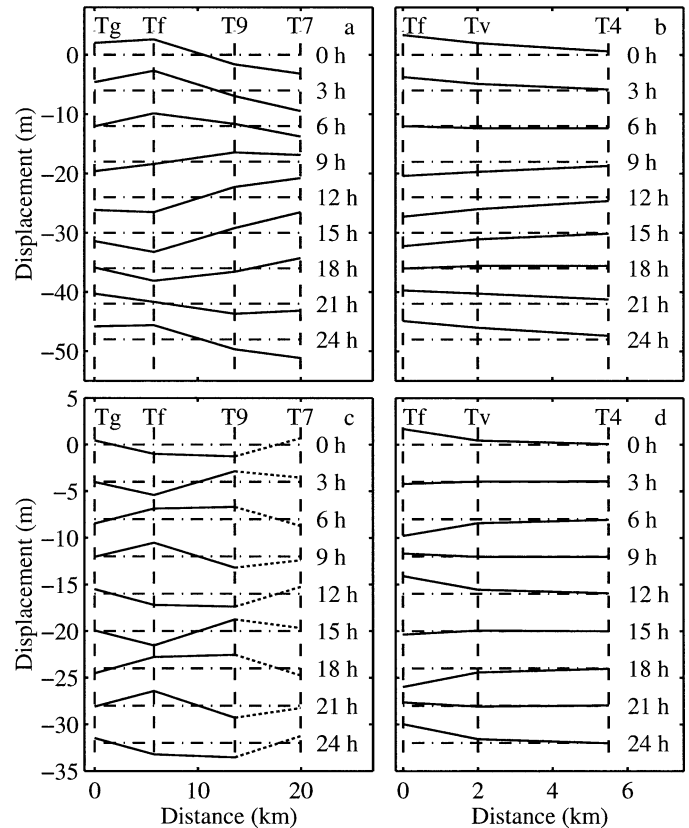


Fig. 7. Temporal evolution of the 24-h component of the 23°C isotherm vertical displacement along the (a) azimuthal and (b) radial direction, and of the 12-h-period component along the (c) azimuthal and (d) radial direction. Solid lines suggest the isotherm displacements from equilibrium position (horizontal dash-dot lines) from data available at the stations (vertical dashed lines) and are replaced by dotted lines where the structure does not resemble an azimuthal mode 1 wave propagating around the whole basin. The numbers on the right of each panel indicate time from the first transect, which is at day 177.71 in panel (a), 177.82 in panel (b), day 177.98 in panel (c), and day 177.81 in panel (d). Each isotherm and its equilibrium position are offset by -6 m in panels (a) and (b) and by -4 m in panels (c) and (d).

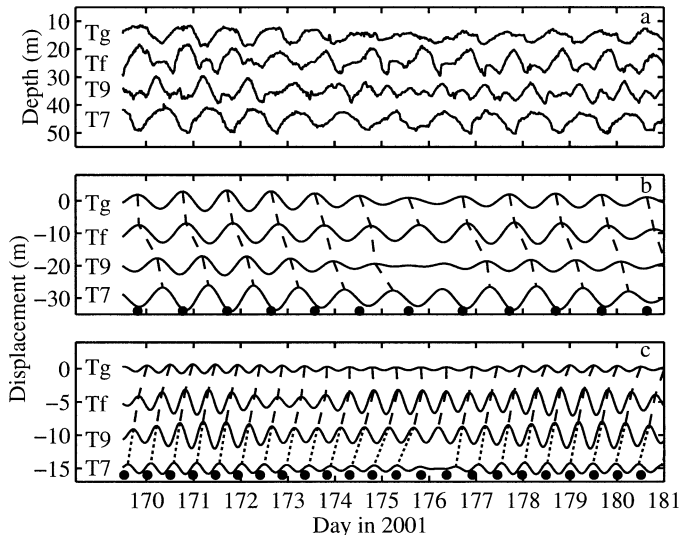


Fig. 6. (a) Depth of the 23°C isotherm displacements at stations along the 20-m isobath (with 10 m offset). Vertical displacement band-passed around (b) 24 h (-10 m offset) and (c) 12 h (-5 m offset). Dashed lines indicate the propagation of the crests of the band-passed signals and are replaced by dotted lines where the suggested propagation does not agree with an azimuthal mode 1 wave propagating around the whole basin. The filled circles toward the bottom of panels (b) and (c) are situated at times where there is a crest at station Tg and are plotted to illustrate the phase lag between stations Tg and T7.

signals of the 23°C isotherm at the stations located along the 20-m-depth contour. The evolution of the 24-h component (Fig. 7a) resembles the cyclonic propagation of an azimuthal mode 1 wave covering the entire basin. The 12-h component (Fig. 7c) appeared to be of an azimuthal mode 2 wave propagating anticyclonically around the basin with oscillations at stations Tg and T7 in phase. However, data recorded at five stations along a west–east transect in 1999 (not shown) suggest that the 12-h component was azimuthal mode 1, as does the transect T9–Tf–Tg in Fig. 7c. This leads to the hypothesis that the structure of the 12-h oscillation was dominated by an azimuthal mode 1 cell in the main part of the basin that did not reach the southern embayment of the basin where station T7 was located.

Radial structure—The phase along a radial transect defined by stations Tf, Tv, and T4 and the monotonic decrease of amplitude with distance from the shore (Fig. 7b,d) indi-

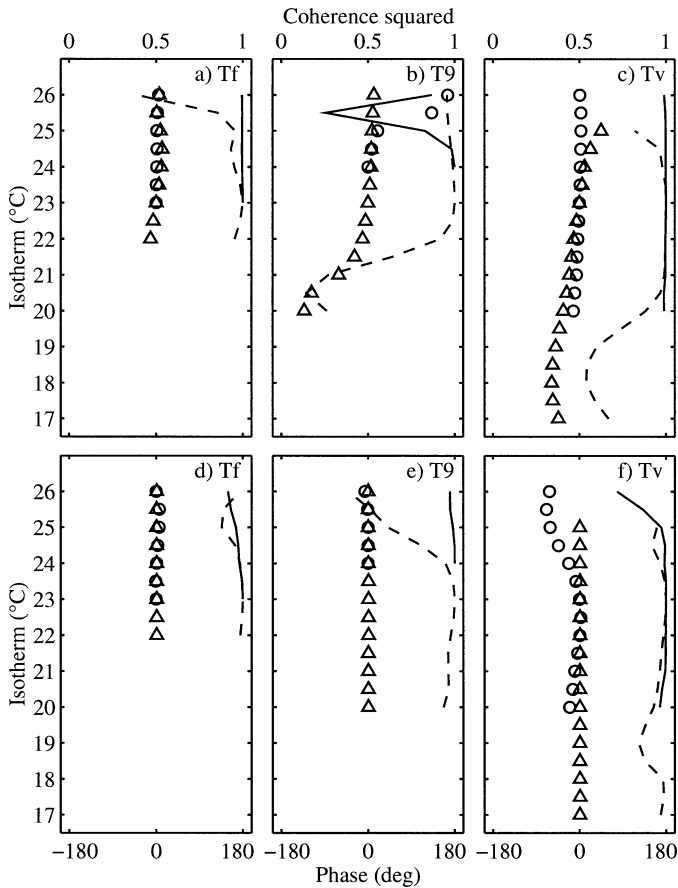


Fig. 8. Profiles of coherence squared (solid line for field data and dashed line for ELCOM results) and phase (circles for field data and triangles for ELCOM results) of the vertical displacement of 24-h (a, b, and c) and 12-h (d, e, and f) period oscillations. Coherence and phase are relative to the 23°C isotherm.

cate that the two dominant components of the wave field were of the first radial mode.

Vertical structure—The vertical modal structure of the 24- and 12-h-period oscillations was identified by calculating the phase of the vertical displacement over the depth of the thermistor chains. The 23°C isotherm was chosen as reference for the phase and the areas where the isotherms intersected the bottom, at any time, were excluded from the analysis. Figure 8 shows the results at those stations where the amplitude of both the 24- and 12-h oscillations were large enough to make the coherence and phase statistically significant. The small change in phase over the water column indicates that a vertical mode 1 dominated both periodic components.

The cyclonic propagation of phase of the 24-h motion and its horizontal and vertical spatial structure suggests that the motion was a Kelvin wave with a vertical and horizontal mode 1 structure that extended over the whole basin, analogous to that for a circular (Antenucci et al. 2000) or elliptical (Antenucci and Imberger 2001) basin shape; the bathymetry did not influence the modality of this wave. In contrast, the bathymetry appeared to have a dramatic influ-

ence on the modal structure of the 12-h wave, the field data suggesting a vertical mode 1 wave with a horizontal structure with two cells. The first cell, in the main part of the basin, seems to have a radial and azimuthal mode 1 structure with anticyclonic propagation of phase; the structure of the second cell, located in the embayment in the south, could not be resolved with the field data and was examined using three-dimensional numerical simulations.

Numerical simulations

We carried out numerical simulations with the Estuary and Lake Computer Model (ELCOM) to increase the spatial resolution of the temperature information and to derive the velocity field. Only a brief description of the model is given here and the reader is referred, for further details, to the original publications by Hodges et al. (2000). The model solves the 3-D, hydrostatic, Boussinesq, Reynolds-averaged Navier–Stokes equations, and scalar transport equations of potential temperature, salinity, and tracers in a Z-coordinate system. Diffusion and advection are separated both for momentum and scalars and a mixing model, based on the integral solution of the turbulent kinetic energy equation, is used to estimate the vertical diffusive transport (Simanjuntak pers. comm.). The model also includes a filter to control the numerical diffusion of potential energy (Laval et al. 2003a), so the stratification and the phase speed of the internal waves are not altered numerically over the simulation period. Heat and momentum exchange at the water surface was estimated by bulk transfer models (e.g., Amorochio and DeVries 1980; Imberger and Patterson 1981; Jacquet 1983), the transfer coefficient being corrected for the stability of the atmospheric boundary layer (Hicks 1975). The surface-energy fluxes are separated into a nonpenetrating component introduced in the surface mixed layer, and a penetrating component introduced over one or more layers according to Beer’s law. Validations with temperature (Hodges et al. 2000; Laval et al. 2003a) and with velocity data (Marti pers. comm.) showed that ELCOM reproduces well the internal wave dynamics in Lake Kinneret. Before using the model to investigate the effect of the bathymetry on the structure of the natural modes, we tested its ability to reproduce the propagation and vertical structure of the dominant observed oscillations for the 2001 data set.

Validation—The bathymetry of the lake was discretized with a 400- × 400- × 1-m grid, and a time step of 450 s was used to satisfy the Courant-Friedrichs-Levy stability condition for the internal motions. Short wave radiation, net radiation, air temperature, and relative humidity inputs were averaged every 10 min from direct measurements taken every 10 s at the meteorological station Ty. A two-dimensional wind field was obtained through spatial linear interpolation of the records from the stations in and around the lake (see Fig. 1). More details about the interpolation of the spatially variable wind may be found in Laval et al. (2003b). The initial temperature profile is taken from Fig. 5a and is considered horizontally homogeneous over the lake.

The spectra in Fig. 4 demonstrate that the model reproduced the concentration of energy at periods of 24 and 12

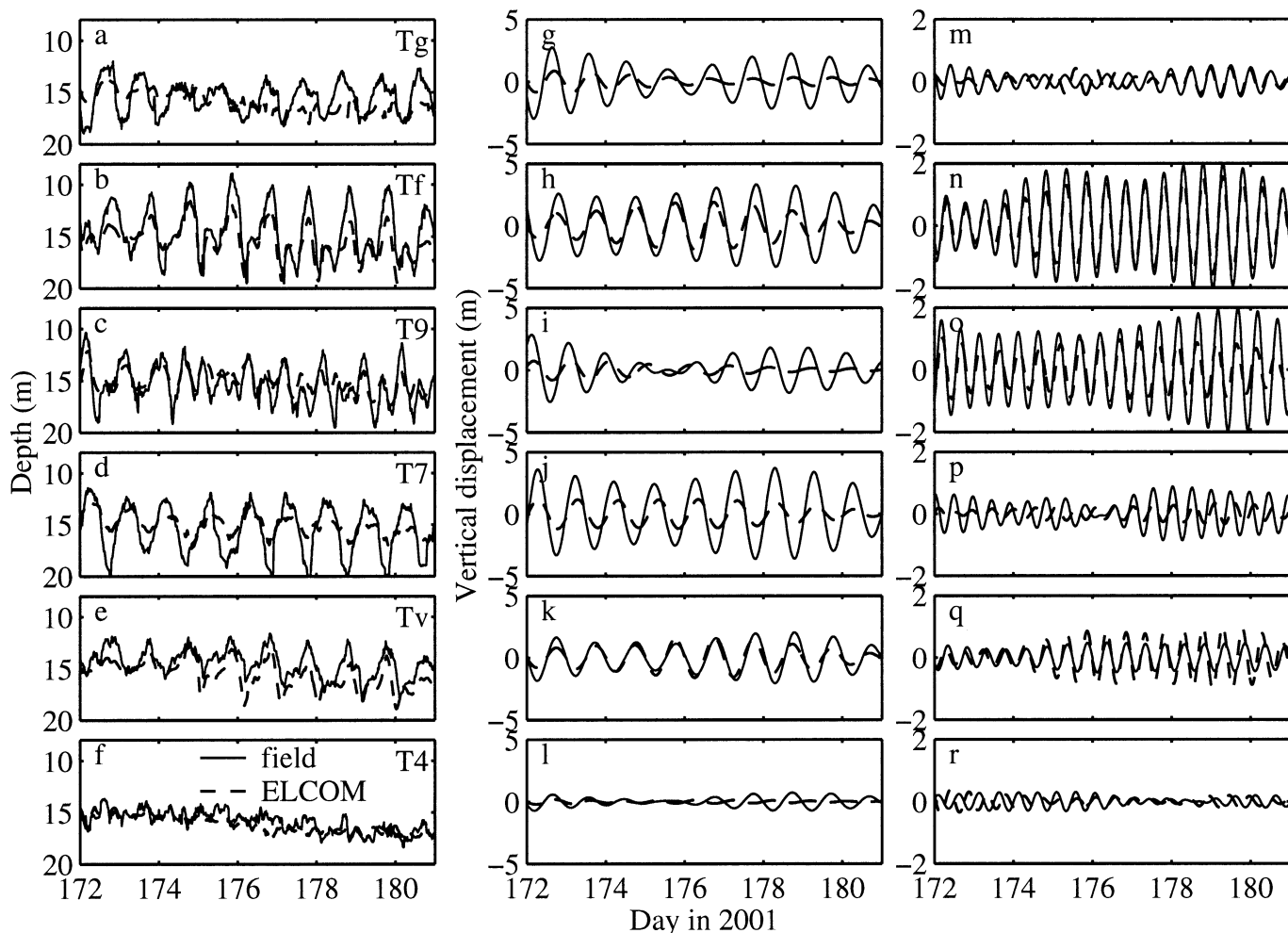


Fig. 9. (a–f) Depth of the 23°C isotherm from field data and ELCOM simulation; (g–l) 23°C isotherm vertical displacements band-pass filtered around 24 h; (m–r) vertical displacements band-pass filtered around 12 h.

h. Figure 9 shows the time series of the 23°C isotherm displacement and its band-pass-filtered components at the six stations. It reveals that the model underestimated, by about 20%, the amplitude of the 24-h component, but simulated well its phase, except at station T4, where the small amplitude of the oscillation made the coherence and phase analysis statistically not significant. We show below that the underestimation of the amplitude was due to artificial dissipation introduced by the no-normal-flow boundary condition applied on the step-like bottom discretization, and that this weakness of the model does not affect the phase and the modal structure of the simulated waves. The phase of the 12-h component was also well simulated at the stations away from the north–south axis (Tf, Tv, and T9), where the coherence and phase analysis were statistically significant. The ability of the model to reproduce their propagation around the basin is verified through an analysis of coherence and phase. The results are summarized in Table 2 and show that both periodic signals were coherent in the stations around the basin in the field measurements and also in the model results. The model results were also coherent with the field data at most of the stations. The cyclonic propagation of

phase of the 24-h signal from Tg to T7 and anticyclonic propagation of phase for the 12-h signal from T9 to Tg were reproduced well by the model, with relatively small differences of both components between the model and the field data. Model results were almost out of phase with field data at T4, but these results were statistically not significant. Excluding T4, the station where the biggest relative phase difference occurred for both signals was T7, the difference being 1.7 h (7% of the observed period) for the 24-h signal and 2 h (17%) for the 12-h signal.

The vertical structure of the model results was analyzed by calculating the phase of the isotherm displacements over the depth of the simulation grid at locations equivalent to those of the thermistor chains. The results (Fig. 8) reproduced well the dominant vertical mode 1 structure of both periodic components observed in the field data. Higher vertical modes might still be present in both the field data and the simulation results, but due to the smaller potential-to-kinetic energy ratio associated with these modes (Antenucci and Imberger 2001), they did not contribute significantly to the isotherm displacement.

Numerical damping in ELCOM: To show that the extra

Table 2. Results of coherence and phase for 23°C-isotherm vertical displacement for field data and ELCOM results. Station Tf is selected as reference for zero phase when LDS or ELCOM results are analyzed independently. When LDS and ELCOM results are compared, LDS data are taken as reference.

Station	LDS (compared with Tf)				ELCOM (compared with Tf)				LDS–ELCOM comparison			
	Phase 24 h		Phase 12 h		Phase 24 h		Phase 12 h		Phase 24 h		Phase 12 h	
	Coh ² 24 h	(°)	Coh ² 12 h	(°)	Coh ² 24 h	(°)	Coh ² 12 h	(°)	Coh ² 24 h	(°)	Coh ² 12 h	(°)
Tg	1.00	−55	0.47	91	0.94	−31	0.88	131	0.89	4	0.18	24
Tf	1.00	0	1.00	0	1.00	0	1.00	0	0.98	−19	0.99	−11
T9	1.00	114	0.94	−111	0.81	136	0.98	−98	0.72	6	0.89	3
T7	0.99	116	0.81	110	0.99	−151	0.95	−179	0.97	25	0.96	60
Tv	0.98	−11	0.98	14	1.00	−2	0.99	−6	0.96	−10	0.97	−31
T4	0.92	−40	0.93	−129	0.75	−179	0.92	103	0.72	−146	0.89	−134

damping in the ELCOM was due to the step bathymetry, we estimated the decay rate of the oscillations in the field and in the model and calculated the relative amplitude of resonant oscillations in two oscillating systems with the different decay rates. The decay rate in ELCOM was estimated by visually fitting a decaying exponential envelope curve to oscillations that follow the release of a tilted stratification in runs with different grid sizes. The associated e-folding times are compared in Table 3. The same procedure could not be applied to the field data, as the lake was forced continuously by the wind before any decay could be evaluated. Instead, we determined the decay rate and the natural period of the Kelvin wave (the most energetic wave) by matching the 24-h band-pass-filtered oscillation of the 23°C isotherm at Tv to the oscillation of a linear damped forced mass-spring system. This simple dynamic system describes the oscillations at a particular location of a lake without the complexity added by the spatial structure (Stocker and Imberger 2003a). The forcing, F , is given by the input of wind momentum approximated by 30-min-long uniform wind blocks. In turn, each constant wind block was considered as made up of a suddenly imposed steady wind event of infinite duration and an equal but negative wind event starting 30 min later. At a particular location in the basin, the isotherm oscillation generated by every wind event (positive or negative) is given by

$$x_i = AF_i \{1 - \cos[\omega(t - t_{\text{lag}})]e^{-\alpha(t-t_{\text{lag}})}\}H(t) \quad (1)$$

where

Table 3. Estimates of dissipation time scale, damped natural period, and resonant amplitude obtained from the field data and from simulations with different grid size. Vwall is the simulation in a basin with flat bottom and the horizontal shape of the perimeter of Lake Kinneret at the depth of the thermocline. The resonant amplitude was nondimensionalized by the resonant amplitude estimated with the field parameters, B_F .

Case	$1/\alpha$ (d)	T (h)	B/B_F
Field	3.9	22.61	1
Vwall	3.4	22.62	0.96
100×100 m	2.8	22.63	0.89
200×200 m	2.2	22.65	0.79
400×400 m	2.1	22.65	0.77

$$\alpha = -\frac{c}{2m}, \quad \omega^2 = \omega_0^2 - \alpha^2 \quad (2)$$

x is the displacement from the equilibrium position, t is the elapsed time from the start of the wind, c is the effective damping coefficient, the coefficient A and the phase t_{lag} account for the spatial location and H is the unit step function. The parameter α is the inverse of the e-folding time, ω is the damped natural frequency, and ω_0 is the undamped natural frequency of the system. The displacement generated by the wind series is given by linear superposition:

$$X(t, \alpha, \omega, A, t_{\text{lag}}) = \sum_{i=1}^M x_i(t - t_{si}) \quad (3)$$

where t_{si} is the time of start of the i th wind event and M is the total number of positive and negative wind events. The values of α and ω were obtained by least-squared fitting X with the 24-h band-pass-filtered 23°C oscillation at station Tv. The 3.9-d decay time scale for the amplitude of the Kelvin wave, α , translates into an energy decay time scale of 2 d, which is about half that estimated by Antenucci and Imberger (2001). This value is also well below the 11.6 d estimated from the experimental results of Wake et al. (2005) in a two-layer, flat-bottom circular basin with the Burger number and inertial period similar to that found in Lake Kinneret, where the transference of energy to smaller scales is limited by the absence of topographic features. From the natural frequency, ω , a natural period of 22.6 h (see Table 3) was calculated for the free Kelvin wave.

Using Eq. 2, we estimated ω_0 , leading to an associated natural period in the absence of damping, T_0 , of 22.59 h. With ω_0 and the different decaying rates, we estimated ω for several grid sizes; the associated periods (Table 3) reveal that the effect of the extra damping on the damped natural period was minor. Although the propagation speed of the simulated Kelvin wave depends on the grid size (Bennett 1977; Beletsky et al. 1997), the effect is practically eliminated if, as in all our simulations, the grid size is less than about one fifth of the internal radius of deformation (Schwab and Beletsky 1998).

The resonant amplitude of the long-term oscillation excited by a harmonic force of amplitude A_F and frequency ω_F , given by

$$B = A_F m^{-1}[(\omega_0^2 - \omega_F^2)^2 + 4\alpha^2\omega_F^2]^{-0.5} \quad (4)$$

(Table 3) shows a 23% reduction of amplitude for the 400×400 grid when the forcing period is 24 h. This is representative of what is observed in Fig. 9, indicating that the smaller amplitude in the model is an effect of grid-step damping.

From the above, we conclude that, despite numerical damping, the model provides a valuable tool to expand the characterization of the modal shape of the isotherm displacements that are induced by the dominant basin-scale internal waves.

Basin with flat bottom and irregular horizontal shape—

We took the analytical solution for the Kelvin and Poincaré natural modes in a circular flat-bottom basin (Csanady 1967, 1972; Antenucci et al. 2000) as the starting point in our investigation of the effects of the irregular bathymetry on the shape of the natural modes. For elliptical basins, Antenucci and Imberger (2001) demonstrated that azimuthal mode 1 Kelvin waves have maximum isotherm displacements where the radius of curvature of the basin is minimum and larger velocities where the radius of curvature is smaller. This behavior is reversed for Poincaré waves.

To look at the effect of the more irregular basin perimeter, we carried out a simulation in an idealized 30-m-deep basin with flat bottom, the horizontal shape of the 15 m depth (mean depth of the thermocline) contour in Lake Kinneret (Fig. 1) and the stratification of the top 30 m of the time-averaged temperature profile in Fig. 5a. A $400 \times 400 \times 1$ -m grid and a 450-s time step were used. The thermodynamic module in ELCOM was switched off and no wind forcing was applied, allowing the system to oscillate freely from an initial west–east tilt of the stratification. Temperature and horizontal velocity time series were recorded at every grid point and used to calculate isotherm displacements and isopycnal velocities time series. The PSD and rotary-power spectral density (RPSD; Gonella 1972) of these time series were then calculated and used to identify spatial variations in the amplitude of the oscillations. The PSD and RPSD revealed dominant periodicities close to 23 and 10.5 h for the vertical displacements and isopycnal velocity. Figure 10 shows the energies of the PSD of vertical displacement and of the RPSD of isopycnal velocities for isotherms in the epilimnion (26.5°C), metalimnion (23°C), and hypolimnion (17°C). The 23-h signal has the characteristics of an azimuthal and vertical mode 1 wave: larger displacements toward the shore (Fig. 10a), especially in the metalimnion, and larger cyclonic velocity component in the epilimnion and hypolimnion with almost no motion in the metalimnion (Fig. 10b). The elongated shape of the lake produced an increase of the vertical displacement where the radius of curvature was minimum and an increase of the velocities where the radius of curvature was maximum, similar to that found for an elliptical basin by Antenucci and Imberger (2001). The vertical displacement of the 10.5-h-period wave was larger toward the perimeter, especially at three locations in the northwest, east, and southwest (Fig. 10c), while two amphidroms were located in the middle of the basin and in the southern embayment. Figure 10d shows the difference between the anticyclonic and cyclonic components of the velocity at 10.5 h. Positive values indicate anticyclonic (clock-

wise) rotation; negative values, cyclonic (anticlockwise) rotation. Two vertical mode 1 counter-rotating cells combined to make the horizontal structure. The first cell filled the main body of the basin and had a classic Poincaré-type structure with velocity vectors rotating anticyclonically and the largest magnitude in the center. In the second cell, located in the embayment in the south of the basin, the velocity vectors rotated cyclonically. The location of Station T7 in the southern cell (Figs. 1, 10d) thus explains why we did not observe a simple structure in the field data when investigating the propagation of phase around the entire basin.

Lake bathymetry with variable depth—

To include the effect of the sloping bottom on the spatial structure of the natural modes of oscillation, we simulated the motion following an initial tilt of the stratification with the real bathymetry of the lake; all other simulation variables were kept the same. The energies of the PSD and RPSD at the dominant periods of 23 and 10.5 h are presented in Fig. 11. All those areas where the isotherms intersected the bottom at any time were excluded from the PSD and RPSD plots, so details of the structure close to the edges of the lake were lost. Despite this, some features still provide an insight of the effects of the sloping bottom on the structure of the natural modes. The 23-h-period wave had larger energy (PSD) of the 23°C isotherm displacements toward the north and south edges of the basin (Fig. 11a) similar to the flat-bottom, irregular horizontal-shape case. In the hypolimnion, in contrast with the small displacements observed for the flat-bottom case, large vertical displacements occurred over the mild bottom slopes in the south and the west of the lake, revealing an intensification of the motion over the sloping bottom. In the hypolimnion (17°C isotherm), the cyclonic component of the RPSD of velocity at 23-h (Fig. 11b) was also larger toward the south and west. Intensification of the isotherm vertical displacement and isopycnal velocity over the sloping bottom also occurred for the 10.5-h-period wave (Fig. 11c,d). The circular Poincaré-type structure of flat-bottom basins with larger velocities in the middle of the cell was retained in the epilimnion (26.5°C isotherm). The two-cell structure of this mode was difficult to observe for the sloping-bottom case because the resolution of the method, as mentioned above, was not sufficient close to the boundary. However, a curtain along the north–south axis of the lake (Fig. 12) shows the anticyclonic rotation of the velocity in the main part of the basin and the cyclonic rotation in the south end. The vertical mode 1 was maintained, but the surface that separates the two cells was tilted.

Interaction of the wind and the dominant natural modes

The field observations reveal that the observed dominant periods in the isotherm displacement are the dominant periods in the forcing and not the period of the natural modes (Figs. 2c and 4). We suggest that the observed oscillations result from the superposition of the free internal waves that are generated by successive wind events. Here, we illustrate how superposition of natural modes explains the effects of the daily changing wind pattern on the observed oscillations.

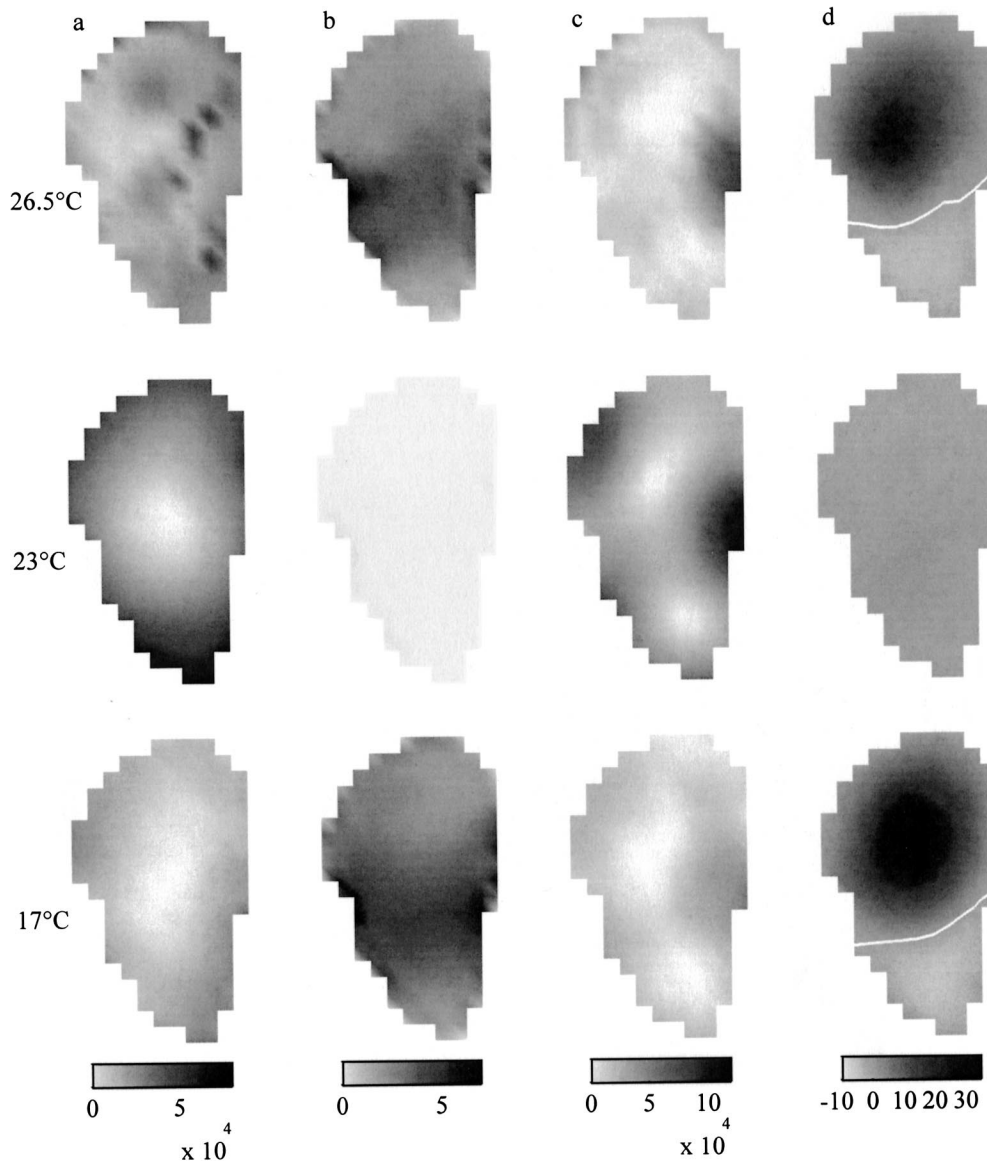


Fig. 10. Dominant natural modes of a basin with the horizontal shape of lake Kinneret 15-m isobath, flat bottom, and continuous stratification. (a) Power spectra of isotherm displacement and (b) cyclonic component of the rotary power spectra of isopycnal velocity for the 23-h-period natural mode; (c) power spectra of isotherm displacement and (d) difference between the anticyclonic and cyclonic components of the rotary power spectra of isopycnal velocity for the 10.5-h-period natural mode (white lines separate zones with opposite rotation). From top to bottom, the rows show results for the 26.5°C, 23°C, and 17°C isotherms, located in the epilimnion, metalimnion, and hypolimnion, respectively. The units of power spectra of vertical displacement are $\text{m}^2 \text{Hz}^{-1}$ and the units of rotary power spectra of isopycnal velocity are $\text{m}^2 \text{s}^{-2} \text{Hz}^{-1}$.

Reset of the phase and modification of the period—With each onset of the wind (Fig. 13a), epilimnetic water started to move to the southeast, the wind forcing it eastward and the Ekman transport turning the flow southward, creating upwelling in the Northwest between stations Tf and Tg (see also Ou and Bennett 1979). At Tf, downwelling of the 23°C isotherm changed into upwelling with the onset of the wind on days 170 and 177; on days 171 and 173–176, the isotherm was already rising at the time of the onset of the wind,

but the rate of upwelling increased when the wind started (Fig. 13b). While the wind was pushing the surface water eastward, a thermocline slope across the basin was built with associated upwelling at Tf and downwelling at T7 (Fig. 13b,c), adding to the one set up by the existing wave field. Regardless of the phase of the preceding wave field, a new set of waves was released at the end of every wind event: strong downwelling at Tf and upwelling at T7 began when the wind fell below 5 m s^{-1} (Fig. 13b,c). The new set of

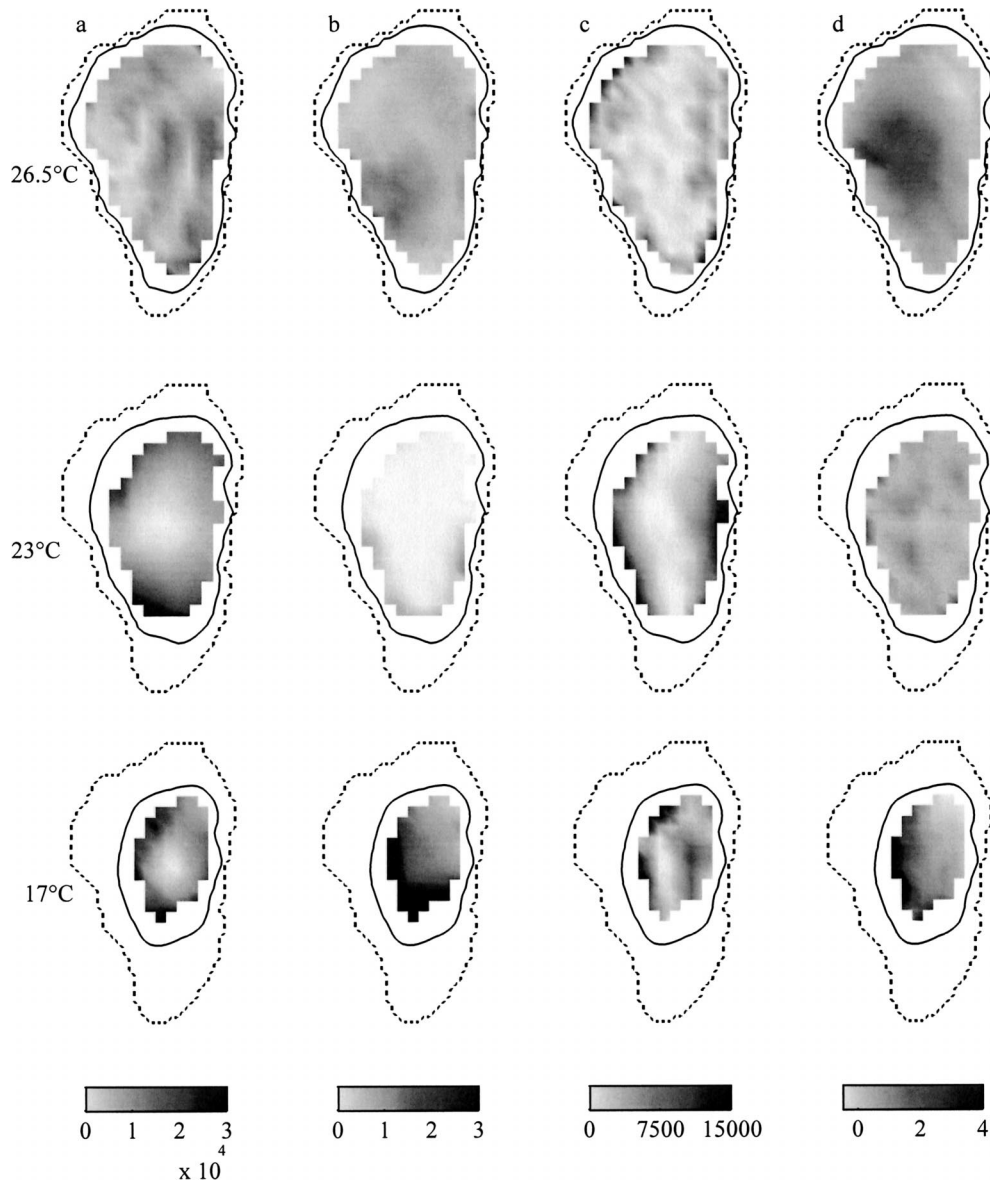


Fig. 11. Dominant natural modes of lake Kinneret. (a) Power spectra of isotherm displacement and (b) cyclonic component of the rotary power spectra of isopycnal velocity for the 23-h-period natural mode; (c) power spectra of isotherm displacement and (d) difference between the anticyclonic and cyclonic components of the rotary power spectra of isopycnal velocity for the 10.5-h-period natural mode. From top to bottom, the rows show results for the 26.5°C, 23°C, and 17°C isotherms, located in the epilimnion, metalimnion, and hypolimnion, respectively. The units of power spectra of vertical displacement are $\text{m}^2 \text{Hz}^{-1}$ and the units of rotary power spectra of isopycnal velocity are $\text{m}^2 \text{s}^{-2} \text{Hz}^{-1}$. The dotted and solid lines show the perimeter of the lake at the levels of the free surface and of the indicated isotherm.

waves released at the end of every wind event added to the waves already propagating around the lake and the combination appears as a reset of the phase of the observed wave field and overrides the natural period of 22.6 h, with the mean forcing period of 24 h.

Resonance—The effect of the temporal pattern of the wind on the wind–wave field interaction was investigated using

extended records between days 169–205 (18 June–24 July) at stations Tg, Tf, and T7. We concentrated on the most energetic 24-h signal. The parameters determining the amplitude of a forced oscillating system are the magnitude of the forcing, the forcing to natural periods ratio, and the actual-to-critical damping coefficients ratio (Norton 1989). In general, lakes are underdamped oscillating systems (Mortimer 1974), for which the maximum resonant amplitude is

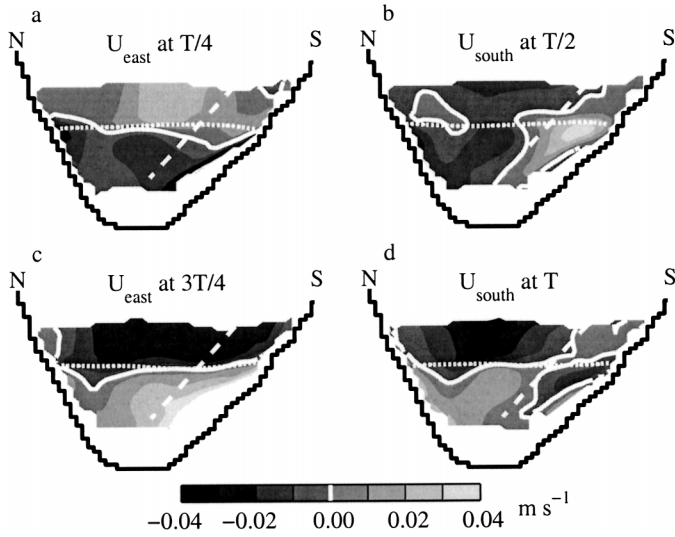


Fig. 12. Snapshots of the relevant component of the 10.5-h band-passed velocity along the north-south axis of Lake Kinneret. (a) and (c) show velocity perpendicular to the transect, with positive values indicating velocities toward the east; (b) and (d), velocity along the transect with positive values indicating velocities toward the south. Solid white lines indicate zero velocity, dotted white lines show the position of the 10.5-h band-passed 23°C-isotherm oscillation, and dashed white lines suggest the location of the boundary between the two counterrotating cells.

reached when the forcing to natural periods ratio approaches one (Norton 1989). The magnitude of the forcing is given by the input of momentum from the wind,

$$\text{Imp} = \frac{1}{\rho} \int_{t_s}^{t_e} \tau dt \quad (5)$$

where

$$\tau = C_D \rho_{\text{air}} U |U| \quad (6)$$

is the shear stress over the water surface, t_s and t_e are start and end times of the wind event, ρ is the water density, t is time, C_D is a drag coefficient, ρ_{air} is the air density, and U is the east component of the wind velocity at Tf. As a new set of waves is released at the end of each wind event, we considered the time from the end of the previous wind event to the end of the wind event under examination, Δt , as the local period of the forcing. The daily variability in the characteristics of the wind forcing and amplitude and time of the peak of the 24-h signal at Tg, Tf, and T7 is presented in Fig. 14.

At Tf, the amplitude was about 3 m (Fig. 14d) and the crests reached the station at around 20 h (Fig. 14e) for the period prior to day 190; after that date, the amplitude dropped to values around 1.2 m due to a decrease in the input of wind momentum (Fig. 14a), and the crest reached Tf at about 19 h as a direct result of the earlier termination of the wind events (Fig. 14b). On days 176, 187, and 188, Δt was close to the natural period of the Kelvin wave (Fig. 14c), so the wave being generated was in phase with the wave generated by the previous wind event and hence the amplitude of the internal waves increased (Fig. 14d). The

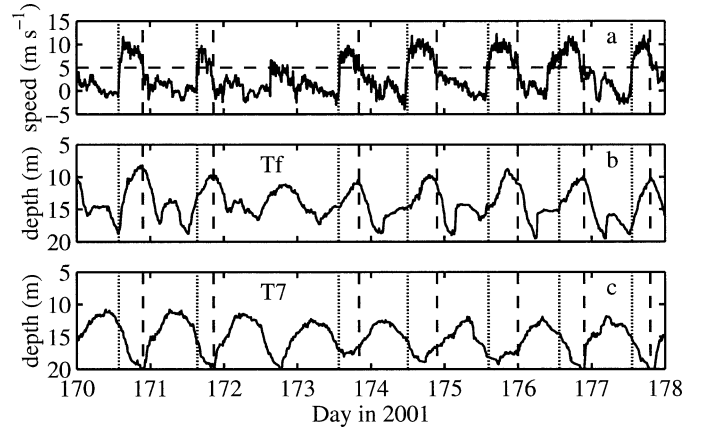


Fig. 13. (a) West-east component of the wind at Tv and depth of the 23°C at stations (b) Tf and (c) T7. Vertical dotted and dashed lines indicate, respectively, the start and the end of wind events.

strong winds on days 174, 175, 185, and 190 did not produce large amplitude of the internal wave because Δt was far from that required for resonance.

The gradual positive phase shift of the wave crests (Fig. 14e) was the effect of the natural period of the wave being

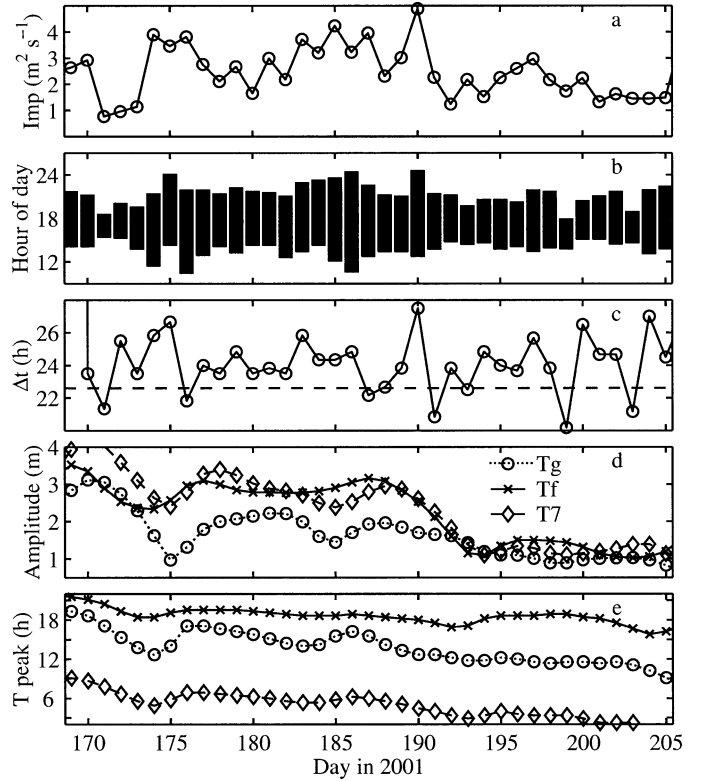


Fig. 14. (a) Momentum input of the daily wind events, (b) temporal location of the daily wind events, (c) elapsed time between the ends of two consecutive daily wind events (the dashed line indicates $\Delta t = 22.6$ h), (d) amplitude of the Kelvin wave, and (e) time of arrival of the Kelvin wave crest. Amplitude and time of arrival of the wave crest are obtained by band-pass filtering around 24 h the 23°C-isotherm displacements.

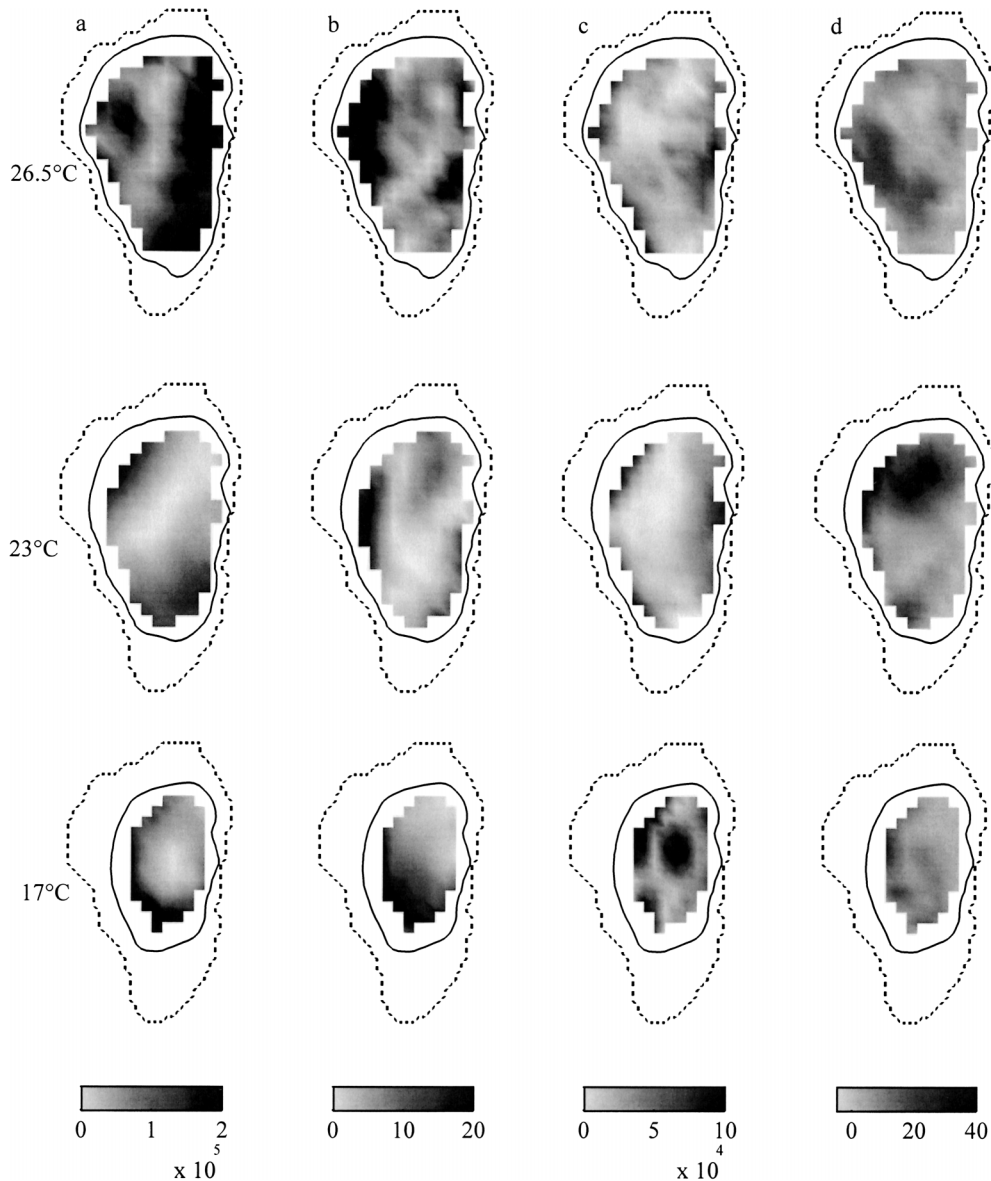


Fig. 15. Lake Kinneret with measured forcing. (a) Power spectra of isotherm displacement and (b) cyclonic component of the rotary power spectra of isopycnal velocity at 24 h; (c) power spectra of isotherm displacement and (d) difference between the anticyclonic and cyclonic components of the rotary power spectra of isopycnal velocity at 12 h. From top to bottom, the rows show results for the 26.5°C, 23°C, and 17°C isotherms, located in the epilimnion, metalimnion, and hypolimnion, respectively. The units of power spectra of vertical displacement are $\text{m}^2 \text{Hz}^{-1}$ and the units of rotary power spectra of isopycnal velocity are $\text{m}^2 \text{s}^{-2} \text{Hz}^{-1}$. The dotted and solid lines show the perimeter of the lake at the levels of the free surface and of the indicated isotherm.

shorter than the average period of the wind and was accentuated when the momentum introduced by the wind was small, as was the case on days 171 to 173. Events of strong wind momentum input generated a negative phase shift (days 174–176, 185–186), especially when the end of the wind event was delayed, as on days 175 and 186.

Spatial structure of the observed oscillations—The spatial structure of the internal wave oscillations observed under atmospheric forcing was extracted from the simulation used

for the validation. The complete structure cannot be visualized because of the lack of resolution of our method close to the bottom, but the results permit the interpretation of the PSD and RPSD as a combination of the signatures of the vertical mode 1 natural modes described above with other motions excited by the wind: The 24-h-period signal (Fig. 15a,b) shows elements of the free Kelvin wave (Fig. 11a,b), such as the larger displacements toward the north and south ends of the lake and the intensification of motion over the sloping bottom in the west. The strong vertical displace-

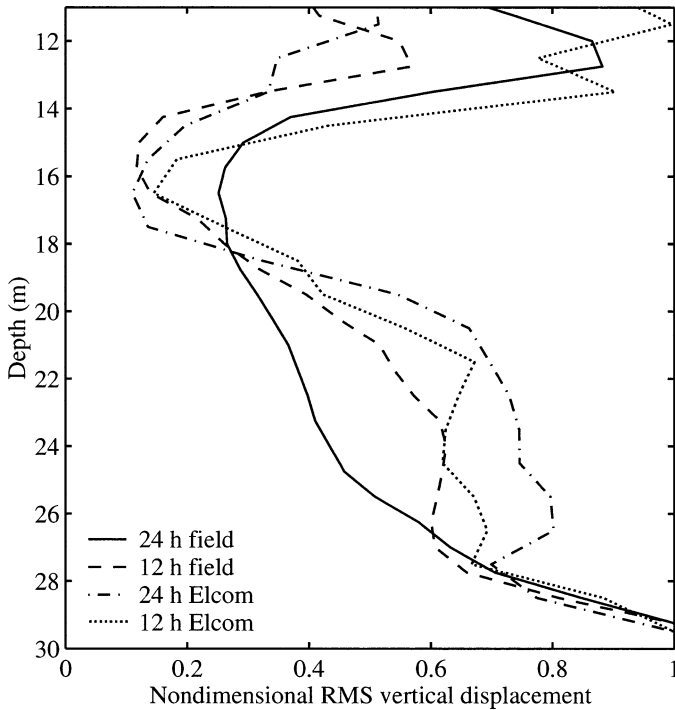


Fig. 16. RMS vertical displacement profile at station Tv calculated from measured and simulated temperature. Profiles are nondimensionalized by the RMS displacement at the most bottom thermistor.

ments observed in the epilimnion at the west and east ends of the lake is the signature of upwelling and downwelling at the ends of a surface layer circulation sustained while the wind was blowing. The 12-h-period signal (Fig. 15c,d) showed strong currents and vertical displacements over the sloping bottom, as in the 10.5-h-period natural mode (Fig. 11c,d). However, additional features in the PSD and RPSD structures suggest that other natural modes with periods close to 12 h were excited. The most noticeable one, a patch of high anticyclonic rotating velocities observed in the metalimnion (23°C isotherm) in the north of the basin, suggests that the wind also excited a vertical mode 2 wave (Lighthill 1978). The existence of this mode is supported by the rotary spectra of velocity data collected close to the location of Tv in 1998 (Antenucci et al. 2000).

The intensification of the velocity over the sloping bottom has, so far, been identified only from model results. We now show that the same slope interaction is seen in the field data by calculating the profile of root mean square (RMS) vertical displacements, s_{rms} , at station Tv (Fig. 16), located on the western slope. To do so, we calculated (following Fricker and Nepf 2000), at the elevation of each thermistor, the time series of temperature fluctuation with respect to the mean temperature profile in Fig. 5 and band passed this at the dominant observed periods, 24 and 12 h. Assuming that changes in temperature are due mainly to vertical displacement (i.e., assuming very small horizontal temperature gradients), the vertical displacement is given by

$$s_{\text{rms}}^j = \frac{\Delta T_{\text{rms}}^j}{\partial T / \partial z} \quad (7)$$

where ΔT_{rms}^j is the RMS temperature fluctuation for the 24-h ($j = 1$) and 12-h ($j = 2$) waves and $\partial T / \partial z$ is the mean temperature vertical gradient. The surface mixed layer is excluded because the temperature fluctuations there are dominated by the heating/cooling diurnal cycle rather than by wave-induced vertical motions. Clearly seen from Fig. 16 is the amplification of the vertical motion over the gently sloping western slope, which is reproduced by ELCOM reasonably well.

Discussion

Temperature data showed that, unlike the Kelvin wave, the 12-h component of the observed oscillations did not have the structure of a wave propagating around the entire basin, pointing to an effect of the irregular bathymetry. Two vertical mode 1 counterrotating cells developed as the result of the plan shape of the basin. This conclusive result embraces previous evidence about the identity of the 12-h signal (Ou and Bennet 1979; Antenucci et al. 2000; Hodges et al. 2000).

There is previous numerical evidence of internal Poincaré waves being locked to some features of the basin (e.g., Wang et al. 2000) and of internal natural modes with a multicellular horizontal structure (Schwab 1977; Lemmin et al. 2005); we offer here a dynamical explanation for their occurrence in terms of the dispersion relationships for circular basins developed by Antenucci and Imberger (2001). The structure of the 21°C isopycnal velocity of the 10.5-h-period wave (Fig. 17) shows circular cells with radii, r_0 , of 4,800 and 3,000 m separated by a no-flow-across vertical curtain. A layered model (Csanady 1982; Monismith 1985) with layer temperatures of 26.5°C, 21.5°C, and 16.5°C and depths of 12.5, 11.0, and 6.5 m gave a first vertical mode phase speed (c_1) of 0.32 m s⁻¹. With f , the local inertia frequency, equal to 7.81×10^{-5} rad s⁻¹, the first vertical mode Burger numbers ($S_1 = c_1 r_0^{-1} f^{-1}$) of the large and small cells were 0.85 and 1.36, respectively. The ratio of the inertial period (22.3 h) to the natural period of this mode (10.5 h) was 2.1. Figure 18a shows how the waves in both cells satisfied the dispersion relationships for azimuthal mode 1 counterrotating Poincaré waves in circular basins. Our results suggest that the horizontal structure of a natural mode has several rotating cells if circular (or elliptic) subbasins holding rotating waves with the same period, vertical and azimuthal modes can geometrically fit into the shape of the basin at the level of the thermocline. The ratio of the radii of the anticyclonic and cyclonic cells coexisting in the horizontal structure of a natural mode, calculated from the dispersion relationships, is thus a useful parameter to predict the existence of counterrotating cells in a natural mode. The ratio for azimuthal mode 1 cells is presented in Fig. 18b as a function of the Burger number of the anticyclonic cell, which is always larger and should occupy the main area of a lake.

Both vertical one natural modes showed a magnification of vertical displacements and velocities over the sloping bottom, similarly to what Münnich (1996) and Fricker and Nepf (2000) found for nonrotating seiches in two-dimensional basins with variable depth. Fricker and Nepf (2000) showed that the magnification of currents and the location of a def-

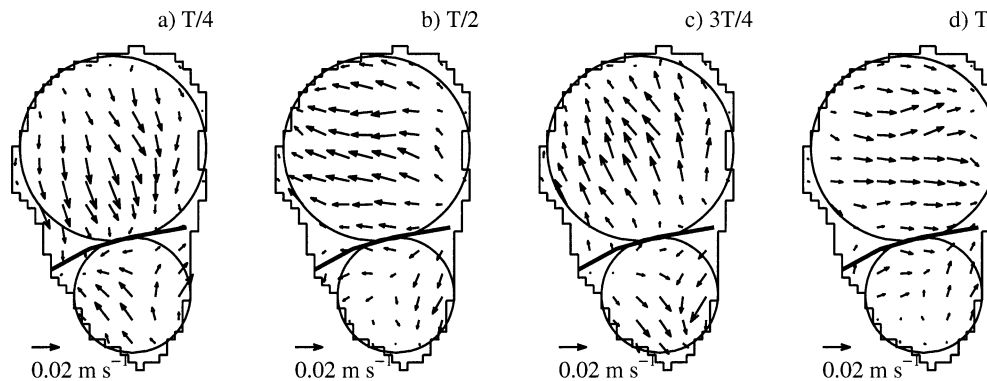


Fig. 17. Snapshots of the 21°C-isothermal velocity for the simulation of the flat-bottom basin with the horizontal shape of the 15-m isobath of lake Kinneret and continuous stratification after an initial tilt. Velocities are band-pass filtered around 10.5 h. The thick line shows a non-cross-flow vertical surface and circles indicate the counterrotating cells.

inite amplitude maximum somewhere over the middle of the slope depends on the structure of the stratification, unlike the flat-bottom case, where the maximum of bed velocity is always located in the middle of the basin. In similar fashion, the maximum bed velocity in the 3-D case is located away from the middle of the cell, where it would occur in a flat-bottom Poincaré wave (Csanady 1967; Antenucci et al. 2000). The amplification of the motion over the sloping bottom suggests that the common use of eigen functions calculated under the assumption of a flat-bottom and negligible vertical bottom velocity (e.g., Monismith 1987; Münnich et al. 1992; Boehrer 2000) should be applied with caution when estimating the vertical structure of the natural modes in lakes.

The intensification of the motion over the sloping bottom may be the result of focusing of internal waves rays after reflection from the lake bed, which is larger if the bottom slope is close to the wave ray slope (the critical slope; Phillips 1966; Dauxois and Young 1999). Despite the step-like structure representation of the bathymetry in ELCOM, the

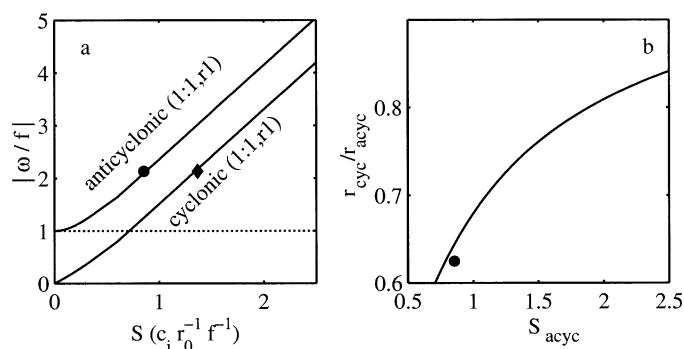


Fig. 18. (a) Dispersion relationships of the two cells of the 10.5-h-period natural mode of a basin with the shape of lake Kinneret at the level of the thermocline, superimposed in the dispersion relationships derived by Antenucci and Imberger (2001). The circle corresponds to the bigger cell in the middle and the diamond corresponds to the smaller cell in the south. (b) Dependence of the ratio of radii of the anticyclonic and cyclonic cells on the Burger number of the anticyclonic cell. The dot indicates the case of Lake Kinneret.

effects of focusing of the wave rays can be simulated, but limited to scales larger than the grid size; the magnitude of the local focusing is better simulated when the slope between bottom cell centers is similar to the real slope.

The slope of the rays of the 10.5-h-period wave at the bottom, s_{gb} , may be estimated from the dispersion relationship for free propagating superinertial internal waves under rotation (LeBlond and Mysak 1978) as

$$s_{gb}^2 = \frac{\omega^2 - f^2}{N_b^2 - \omega^2} \quad (8)$$

where ω is the frequency of the natural mode and N_b is the buoyancy frequency at the bottom of the water column. The interaction with the sloping boundary generates refraction of these waves but the slope of the rays remains unchanged (LeBlond and Mysak 1978). The ray slope of the subinertial internal Kelvin wave cannot be described by Eq. 8. Rhines (1970) showed that, as for internal Kelvin waves propagating along a vertical and straight wall, the dispersion relationship of subinertial internal waves propagating along a wall tilted at any angle from the vertical is that of free internal waves in the absence of rotation. The inertial frequency, f , only influences the trapping of the motion to the wall. Based on these results, we estimated the slope of the rays of the Kelvin wave at the bottom from the dispersion relationship of free waves in the absence of rotation as

$$s_{gb}^2 = \frac{\omega^2}{N_b^2 - \omega^2} \quad (9)$$

As seen from Figs. 19 and 11c,d, the ray slope was similar to the bottom slope close to the areas where intensification of the oscillations was observed in the west and, for the case of the 22.6-h Kelvin wave, in the south. Therefore, it is likely that the observed intensification over the slope was the signature of the propagation of wave rays that were strongly focused after reflection in the bottom.

We based our analysis of the observed oscillations in terms of resonant interaction of the wind with the natural modes of the basin. Using geometrical tracing of wave rays, Maas and Lam (1995) showed that, in an inviscid two-dimensional parabolic basin with constant buoyancy frequen-

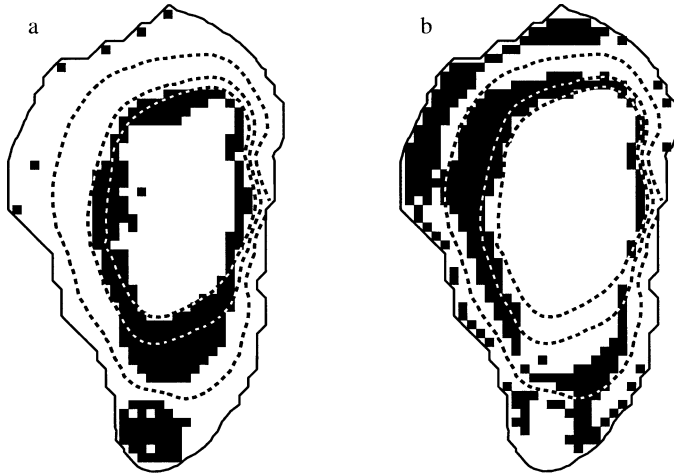


Fig. 19. Shaded areas indicate where the ratio of the bottom and critical slopes is between 1/1.5 and 1.5 for (a) the 22.6-h-period Kelvin natural mode and (b) the 10.5-h-period natural mode. The slope of the wave rays was calculated with Eqs. 8 and 9 with the value buoyancy frequency at the bottom taken from Fig. 5b. Dotted contours indicate the intersection of the 26.5°C, 23°C, and 17°C isotherms mean levels with the bottom of the lake.

cy, wave rays do not close upon themselves and natural modes do not exist. Instead, for some frequencies (and their associated angles of propagation), focusing makes all the wave rays converge toward a fixed trajectory, called an attractor, where all the energy concentrates and coherent modes are no longer observed. For other frequencies, the focusing is balanced by defocusing and the rays do not converge toward an attractor but do not close either, producing what they defined as an infinite period attractor where one ray fills the entire basin. These authors suggest that natural coherent seiching modes in sloping bottom basins are possible only for particular geometries.

Their analysis relies on the geometric construction of the characteristics using the dispersion relationship for linear inviscid internal waves in a medium with constant buoyancy frequency, N , where the angle that the wave ray forms to the horizontal, θ , is maintained after reflection from a slope (Phillips 1966). If viscosity is considered, the resulting dispersion relationship is

$$\omega^2 + i\omega\nu K^2 - N^2\cos^2\theta = 0 \quad (10)$$

where ν is the kinematic viscosity and K is the magnitude of the wave vector (Kistovich and Chashechkin 1995). After reflection, changes in K must then be compensated with changes in θ , especially when focusing of the wave rays produces larger values of K . For low-period attractors, viscous diffusion then balances geometrical focusing of the rays and the motion concentrates in a shear layer around the attracting trajectory, as is shown numerically by Dintrans et al. (1999) and Rieutord et al. (2001). These authors also showed that regular coherent modes are recovered from the infinite-period attractors when viscous diffusion is taken into account.

Münnich (1996) found numerically a V1H1 natural mode in a parabolic basin for which Maas and Lam (1995) ruled

out the existence of any natural mode. Although viscous diffusion was not considered explicitly in Münnich's work, numerical diffusion may have had a similar effect to its physical counterpart, leading to the occurrence of natural modes. Besides viscous diffusion, nonlinear effects (Dauxois and Young 1999; Manders and Maas 2004) and the breakdown of the hydrostatic approximation (Maas 2001) can also invalidate the conclusions in Maas and Lam (1995) about the nonexistence of coherent natural seiching modes. Our data and previous observations (e.g., Thorpe 1974; Lemmin 1987; Münnich et al. 1992) suggest that natural modes of oscillations are ubiquitous in stratified lakes and focusing and defocusing of all internal wave rays must balance to produce wave rays that close upon themselves.

Maas et al. (1997), Maas (2001), and Manders and Maas (2004) demonstrated in the laboratory the existence of shear layers around the predicted trajectory of a low-period attractor. We believe that they are not observed in stratified lakes for several reasons. First, the wind forcing is not a pure harmonic motion (or a simple combination of few pure harmonic motions) sustained for a high number of wave periods, as was always the case in the mentioned experiments. Second, the long forcing time necessary to generate a low-period attractor also indicates that they are highly dissipative and that it is very unlikely that they remain after the forcing ceases. This was observed by Boegman (pers. comm.), who noticed that forced interfacial modes generated by harmonically forcing a two-layer rectangular tank die very quickly after the forcing stops. In addition, the long scale of the wind forcing at the lake surface creates over-specification of the boundary conditions (Maas and Lam 1995) and destroys the attractor. Manders and Maas (2003) reported difficulties to observe attractors when a length scale is imposed by an oscillating paddle.

We described the observed oscillations in Lake Kinneret as the superposition of internal natural modes generated by every wind event, on average, every 24 h rather than as a harmonic forced internal wave with a 24-h period. This representation is more appropriate due to the wind pattern and was successful in explaining the changes in amplitude of the observed oscillations in terms of the resonant interaction of the wind with the dominant natural mode of the basin.

Degeneracy (several natural modes may have the same frequency) and denseness (internal natural modes frequencies may vary over a continuous range) (Münnich 1996) make the concept of natural modes fragile according to Maas and Lam (1995), but we argue that the concept is still valid because the spatial structure of the modes makes them clearly distinguishable and dictates which one of them is excited by a wind with a given horizontal structure.

The azimuthal and vertical mode 1 Kelvin wave, previously identified in Lake Kinneret by Serruya (1975), Ou and Bennett (1979), and Antenucci et al. (2000), was shown to travel around the entire basin and to possess a natural period of 22.6 h, shorter than the observed periodicity of 24 h. The wave amplitude is intensified at the southern and northern extremities of the lake where the radius of curvature is smallest, in agreement with the numerical results of Schwab (1977) for a flat-bottomed Lake Ontario and the analytical

solution for a flat-bottom elliptical basin of Antenucci and Imberger (2001).

The second dominant internal mode was made up of two counterrotating 10.5-h-period Poincaré waves of the first vertical mode that meet the dispersion relationships for circular basins. Once again, this wave was also phase adjusted each day by the wind forcing leading to a spectral peak close to 12 h. The basin shape was shown to have two influences on the wave motion. First, the plan shape determined, through the perimeter radius of curvature, the azimuthal Kelvin wave amplitude variations, smaller radii leading to an amplification of the amplitude. By contrast, the effect on the 10.5-h-period natural mode was to generate the two counterrotating Poincaré cells. Second, a sloping bottom induced an amplification of the horizontal wave velocity over the slope similar to what has previously been predicted in vertical two-dimensional basins; this is likely produced by focusing of internal wave rays. In Lake Kinneret, gently sloping regions have larger bottom velocities and thus higher potential for sediment resuspension. We also showed that the elapsed time between the ends of two consecutive wind events determined whether resonance between the wind and wave motion occurred on a diurnal time scale.

References

- AMOROCHO, J., AND J. J. DEVRIES. 1980. A new evaluation of the wind stress coefficient over water surfaces. *J. Geophys. Res.* **85**: 433–442.
- ANTENUCCI, J. P., AND J. IMBERGER. 2001. Energetics of long internal gravity waves in large lakes. *Limnol. Oceanogr.* **46**: 1760–1773.
- , AND ———. 2003. The seasonal evolution of wind/internal wave resonance in Lake Kinneret. *Limnol. Oceanogr.* **48**: 2055–2061.
- , ———, AND A. SAGGIO. 2000. Seasonal evolution of the basin-scale internal wave field in a stratified lake. *Limnol. Oceanogr.* **45**: 1621–1638.
- BÄUERLE, E. 1998. Excitation on internal seiches by periodic forcing, p. 167–178. *In* J. Imberger [ed.], *Physical processes in lakes and oceans*. Coastal and Estuarine Studies, V. 54. AGU.
- BELETSKY, D., W. P. O'CONNOR, D. J. SCHWAB, AND D. E. DIETRICH. 1997. Numerical simulation of internal Kelvin waves and coastal upwelling fronts. *J. Phys. Oceanogr.* **27**: 1197–1215.
- BENDAT, J., AND A. PERSOL. 1986. *Random data. Analysis and measurement procedures*, 2nd ed. Wiley.
- BENNETT, J. R. 1977. A three-dimensional model of Lake Ontario's summer circulation. I: Comparison with observations. *J. Phys. Oceanogr.* **7**: 591–601.
- BOEGMAN, L., J. IMBERGER, G. N. IVEY, AND J. P. ANTENUCCI. 2003. High frequency internal waves in large stratified lakes. *Limnol. Oceanogr.* **48**: 895–919.
- BOEHRER, B. 2000. Modal response of a deep stratified lake: Western lake Constance. *J. Geophys. Res.* **105**: 28837–28845.
- CSANADY, G. T. 1967. Large-scale motion in the Great Lakes. *J. Geophys. Res.* **72**: 4151–4162.
- . 1972. Response of large stratified lakes to wind. *J. Phys. Oceanogr.* **2**: 3–13.
- . 1982. On the structure of transient upwelling events. *J. Phys. Oceanogr.* **12**: 84–96.
- DAUXOIS, T., AND W. R. YOUNG. 1999. Near-critical reflection of internal waves. *J. Fluid Mech.* **390**: 271–295.
- DINTRANS, B., M. RIEUTORD, AND L. VALDETTARO. 1999. Gravitoinertial waves in a rotating stratified sphere or spherical shell. *J. Fluid Mech.* **398**: 271–297.
- ERIKSEN, C. C. 1982. Observations of internal wave reflections off sloping bottoms. *J. Geophys. Res.* **87**: 525–538.
- FRICKER, P. D., AND H. M. NEPF. 2000. Bathymetry, stratification and internal seiche structure. *J. Geophys. Res.* **105**: 14237–14251.
- GLOOR, M., A. WÜEST, AND M. MÜNNICH. 1994. Benthic boundary mixing and resuspension induced by internal seiches. *Hydrobiologia.* **284**: 59–68.
- GONELLA, J. 1972. A rotary-component method for analysing meteorological and oceanographic vector time series. *Deep Sea Res.* **19**: 833–846.
- HEAPS, N. S., AND A. E. RAMSBOTTOM. 1966. Wind effects on water in a narrow two-layered lake. *Phil. Trans. R. Soc. London, Ser. A* **259**: 391–430.
- HICKS, B. B. 1975. A procedure for the formulation of bulk transfer coefficients over water. *Bound. Layer Meteorol.* **8**: 515–524.
- HODGES, B. R., J. IMBERGER, A. SAGGIO, AND K. B. WINTERS. 2000. Modeling basin-scale internal waves in a stratified lake. *Limnol. Oceanogr.* **45**: 1603–1620.
- IMBERGER, J. 1998. Flux paths in a stratified lake: A review, p. 1–17. *In* J. Imberger [ed.], *Physical processes in lakes and oceans*. Coastal and Estuarine Studies, V. 54. AGU.
- , AND J. C. PATTERSON. 1981. A dynamic reservoir simulation model-DYRESM 5, p. 310–361. *In* H. Fisher [ed.], *Transport models for inland and coastal waters*. Academic.
- IVEY, G. N., AND T. MAXWORTHY. 1992. Mixing driven by internal Kelvin waves in large lakes and the coastal oceans. *Proceedings 11th Australasian Fluid Mechanics Conference*, Hobart, Australia, p. 303–306.
- JACQUET, J. 1983. Simulation of the thermal regime of rivers, p. 150–176. *In* G. T. Orlob [ed.], *Mathematical modelling of water quality: Streams, lakes and reservoirs*. Wiley-Interscience.
- KISTOVICH, Y. V., AND Y. D. CHASHECHKIN. 1995. The reflection of beams of internal gravity waves at a flat rigid surface. *J. Appl. Math. Mech.* **59**: 579–585.
- LAVAL, B., B. R. HODGES, AND J. IMBERGER. 2003a. Numerical diffusion in 3D, hydrostatic, z-level lake models. *J. Hydraul. Eng.* **129**: 215–224.
- , J. IMBERGER, B. R. HODGES, AND R. STOCKER. 2003b. Modeling circulation in lakes: Spatial and temporal variations. *Limnol. Oceanogr.* **48**: 983–994.
- LEBLOND, P. H., AND L. A. MYSAK. 1978. *Waves in the ocean*. Elsevier.
- LEMMIN, U. 1987. The structure and dynamics of internal waves in Baldeggensee. *Limnol. Oceanogr.* **32**: 43–61.
- , C. H. MORTIMER, AND E. BÄUERLE. 2005. Internal seiche dynamics in Lake Geneva. *Limnol. Oceanogr.* **50**: 207–216.
- LIGHTHILL, J. 1978. *Waves in fluids*. Cambridge.
- MAAS, L. R. M. 2001. Wave focusing and ensuing mean flow due to symmetry breaking in rotating fluids. *J. Fluid Mech.* **437**: 13–28.
- , D. BENIELLI, J. SOMMERIA, AND F.-P. A. LAM. 1997. Observation of an internal wave attractor in a confined, stably stratified fluid. *Nature.* **388**: 557–561.
- , AND F.-P. A. LAM. 1995. Geometric focusing of internal waves. *J. Fluid Mech.* **300**: 1–41.
- MANDERS, A. M. M., AND L. R. M. MAAS. 2003. Observations of inertial waves in a rectangular basin with a sloping boundary. *J. Fluid Mech.* **493**: 59–88.
- , AND ———. 2004. On the three-dimensional structure of the inertial wave field in a rectangular basin with one sloping boundary. *Fluid Dyn. Res.* **35**: 1–21.
- MONISMITH, S. G. 1985. Wind-forced motions in stratified lakes and

- their effect on mixed-layer shear. *Limnol. Oceanogr.* **30**: 771–783.
- . 1987. Modal response of reservoirs to wind stress. *J. Hydr. Eng.* **113**: 1290–1306.
- MORTIMER, C. H. 1974. Lake hydrodynamics. *Verh. Int. Ver. Limnol.* **20**: 124–197.
- MÜNNICH, M. 1996. The influence of bottom bathymetry on internal seiches in stratified media. *Dyn. Atmos. Oceans.* **23**: 257–266.
- , A. WÜEST, AND D. M. IMBODEN. 1992. Observations of the second vertical mode of the internal seiche in an alpine lake. *Limnol. Oceanogr.* **37**: 1705–1719.
- NORTON, M. P. 1989. *Fundamentals of noise and vibration analysis for engineers*. Cambridge.
- OSTROVSKY, I., Y. Z. YACOBI, P. WALLINE, AND I. KALIKHMAN. 1996. Seiche-induced mixing: Its impact on lake productivity. *Limnol. Oceanogr.* **41**: 323–332.
- OU, H., AND J. R. BENNETT. 1979. A theory of the mean flow driven by long internal waves in a rotating basin, with application to Lake Kinneret. *J. Phys. Oceanogr.* **9**: 1112–1125.
- PHILLIPS, O. M. 1966. *The dynamics of the upper ocean*. Cambridge University Press.
- RHINES, P. 1970. Edge-, bottom-, and Rossby waves in a rotating stratified fluid. *Geophys. Fluid Dyn.* **1**: 273–302.
- RIEUTORD, M., B. GEORGEOT, AND L. VALDETTARO. 2001. Inertial waves in a rotating spherical shell: Attractors and asymptotic spectrum. *J. Fluid Mech.* **435**: 103–144.
- RUEDA, F. J., S. G. SCHLADOW, AND S. O. PALMARSSON. 2003. Basin-scale internal wave dynamics during a winter cooling period in a large lake. *J. Geophys. Res.* **108**: art. no. 3097.
- SAGGIO, A., AND J. IMBERGER. 1998. Internal wave weather in a stratified lake. *Limnol. Oceanogr.* **43**: 1780–1795.
- SALVADÈ, G., F. ZAMBONI, AND A. BARBIERI. 1988. Three-layer model of the north basin of the lake of Lugano. *Annales Geophysicae.* **6**: 463–474.
- SCHWAB, D. J. 1977. Internal free oscillation in Lake Ontario. *Limnol. Oceanogr.* **22**: 700–708.
- , AND D. BELETSKY. 1998. Propagation of Kelvin waves along irregular coastlines in finite-difference models. *Advances in water resources.* **22**: 239–245.
- SERRUYA, S. 1975. Wind, water temperature and motions in Lake Kinneret: General pattern. *Verh. Int. Ver. Limnol.* **19**: 73–87.
- STOCKER, R., AND J. IMBERGER. 2003a. Energy partitioning and horizontal dispersion in a stratified rotating lake. *J. Phys. Oceanogr.* **33**: 512–529.
- , AND ———. 2003b. Horizontal transport and dispersion in the surface layer of a medium size lake. *Limnol. Oceanogr.* **48**: 971–982.
- THORPE, S. A. 1974. Near-resonant forcing in a shallow two-layer fluid: A model for the internal surge in Loch Ness? *J. Fluid Mech.* **63**: 509–527.
- TURNER, J. S. 1973. *Buoyancy effects in fluids*. Cambridge.
- WAKE, G. W., G. N. IVEY, AND J. IMBERGER. 2005. The temporal evolution of baroclinic basin-scale waves in a rotating circular basin. *J. Fluid Mech.* **523**: 367–392.
- WANG, Y., K. HUTTER, AND E. BÄUERLE. 2000. Wind-induced baroclinic response of Lake Constance. *Ann. Geophysicae.* **18**: 1488–1501.

Received: 10 May 2005

Accepted: 9 July 2005

Amended: 1 September 2005